

1 Sea surface salinity restoring

We compare the ocean circulation after 1000 years of simulation in a LGM spinup with and without extra adjustments to the sea surface salinity (SSS) reference field used for salinity restoring. The adjusted spinup is the one used in our study and described in the main text. If unadjusted, the LGM SSS reference field is derived from the PI SSS reference field through the addition of a PMIP3-based sea surface salinity anomaly (Morée and Schwinger, 2019a; Morée and Schwinger, 2019b) (Fig. S1a). For the unadjusted setup NorESM-OC simulated an AMOC of 21 Sv (17 Sv for the adjusted spinup), and a Drake Passage through flow of 112 Sv (134 Sv for the adjusted spinup). The SSW profoundly decrease their volume in the Atlantic (Fig. S2). As especially the retreat of SSW is in disagreement with proxy-based reconstructions (see main text), we applied an adjustment to the SSS relaxation of -0.5 psu in the North Atlantic in the region where the anomaly was largest, as well as in the Southern Ocean (Fig. S1a). The simulated SSS for the adjusted run is shown in Fig. S1b.

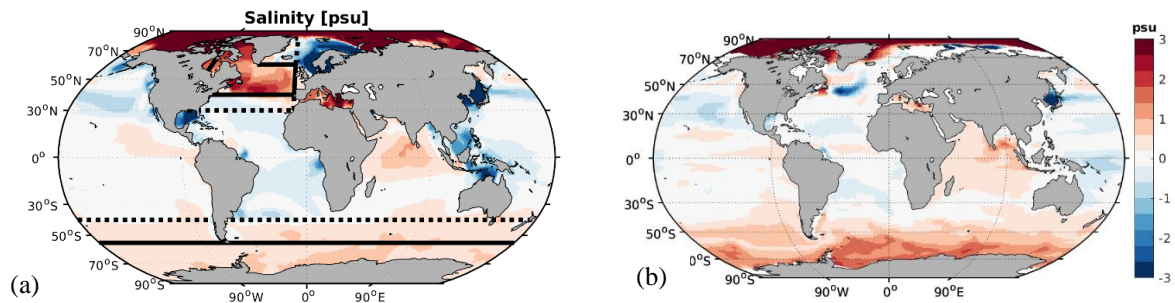


Figure S1 Sea surface salinity anomaly between the LGM and PI, with regions of salinity relaxation adjustment. (a) SSS anomaly in model forcing. In addition, the North Atlantic region, which is decreased by 0.5 psu, extends between 90°W and 45°W from 40°N to 80°N, and between 45°W to 10°W from 40°N to 60°N. The additional anomaly is linearly ramped off to zero at the line along 30°N and to the point 80°N 10°W. In the Southern Ocean, 0.5 psu is added south of 55°S, and ramped off to zero until 40°S. (b) Simulated SSS LGM-PI change.

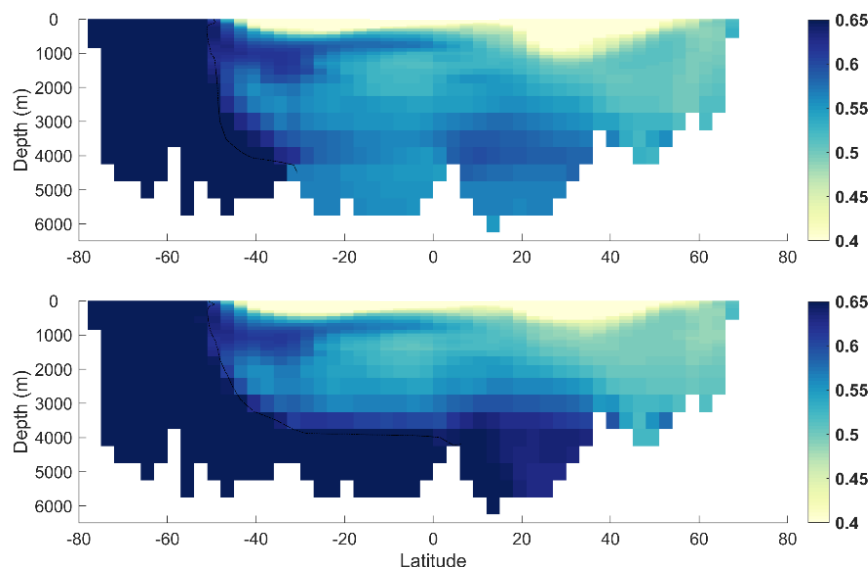


Figure S2 Atlantic PO tracer (as Fig. 1) after 1000 years of spinup without salinity adjustment (upper) and with salinity adjustment (lower).

2 LGM Normal Year Forcing

The PMIP3-based atmospheric anomaly fields which were used to obtain an atmospheric forcing representative of the LGM (Morée and Schwinger, 2019a; Morée and Schwinger, 2019b) received an update (version 2, retrievable in Morée and Schwinger, 2019a) after the model simulations for this study were finished. Version 2 is based on PMIP3 models CNRM-CM5, IPSL-CM5A-LR, GISS-E2-R, MIROC-ESM and MRI-CGCM3 for all variables including SSS. In version 1, GISS-E2-R was not included and the SSS anomaly was based on CNRM-CM5 and MIROC-ESM. We evaluated the differences in the LGM spinup after 500 model years between version 1 and version 2 of these anomaly fields. We note that the modelled circulation is not fully equilibrated yet at this stage, but limit our comparison due to computational costs. We conclude that the SSS tuning applied as described in SM1 is specific to version 1 of the forcing anomaly, and should be adjusted for version 2.

3 Calculation of LGM-PI Δ DIC

We estimate the LGM-PI change in marine DIC content by applying the same approach used to estimate Δ land in Jeltsch-Thömmes et al. (2019). To this end, the forcing-response relationships of seven generic deglacial carbon cycle mechanisms in regard to LGM-PI changes in four observational targets ($p\text{CO}_2^{\text{atm}}$, $\delta^{13}\text{C}^{\text{atm}}$, marine $\delta^{13}\text{C}$ of DIC, or deep equatorial Pacific CO_3^{2-}) and DIC are investigated with the Bern3D Earth System Model of Intermediate Complexity. The seven processes cover physical mechanisms, mechanisms related to oceanic carbonate and organic matter, and changes in the land biosphere carbon inventory (for details please see Jeltsch-Thömmes et al., 2019). These seven generic deglacial carbon cycle mechanisms were varied individually by systematic parameter variations in addition to well-established forcings such as orbital parameters, greenhouse gas radiative forcing, land ice albedo, coral reef regrowth, and North Atlantic freshwater forcing. In a next step, Latin hypercube parameter sampling was used to vary the processes in combination and probe for nonlinear interactions and use the results to adjust the above forcing-response relationships. A simple emulator of the form

$$\Delta T = a^T + b^T * (\sum_{i=1}^7 \Delta p_i * S_i^T),$$

where $S_i^T = \partial T / \partial p_i$ is the sensitivity for each target T to each mechanism i and the corresponding parameter change Δp_i is derived. a^T is the offset and b^T the slope of the respective linear fit from the multi-parameter adjustment. We use the same half a million parameter combinations as used in Jeltsch-Thömmes et al. (2019) and with Δ DIC as target. The four proxy targets ($p\text{CO}_2^{\text{atm}}$, $\delta^{13}\text{C}^{\text{atm}}$, marine $\delta^{13}\text{C}$ of DIC, or deep equatorial Pacific CO_3^{2-}) are used as constraints.

Applying single constraints only, yields similar ranges for Δ DIC for each constraint. Considering all four proxy targets simultaneously shifts the estimate of Δ DIC to higher values (Fig. S3a). We can further disentangle contributions to Δ DIC: Sedimentation-weathering imbalances contribute the most to Δ DIC and with the largest uncertainty (Fig. S3b). The contribution from corals reflects the uncertainty of the estimated amount of coral reef growth. The estimates range from 380 Gt C (Vecsei and Berger, 2004) to 1200 Gt C and more (Milliman, 1993; Kleypas, 1997; Ridgwell et al., 2003). For the discussion of the contribution from the land biosphere the reader is referred to Jeltsch-Thömmes et al. (2019). The atmospheric contribution is a result of the prescribed LGM to PI CO_2 target of 80-100 ppm. The results point to an important role and large contribution from sedimentation-weathering imbalances to Δ DIC estimates over glacial/interglacial timescales, however, with a large uncertainty.

It has to be noted that in order to use the cost-efficient emulator and explore a large parameter space only the change between LGM and PI was considered. Including the spatio-temporal evolution of several proxies in transient model simulations will help to further gain understanding into governing processes and narrow down the Δ DIC estimate but is beyond the scope of this manuscript.

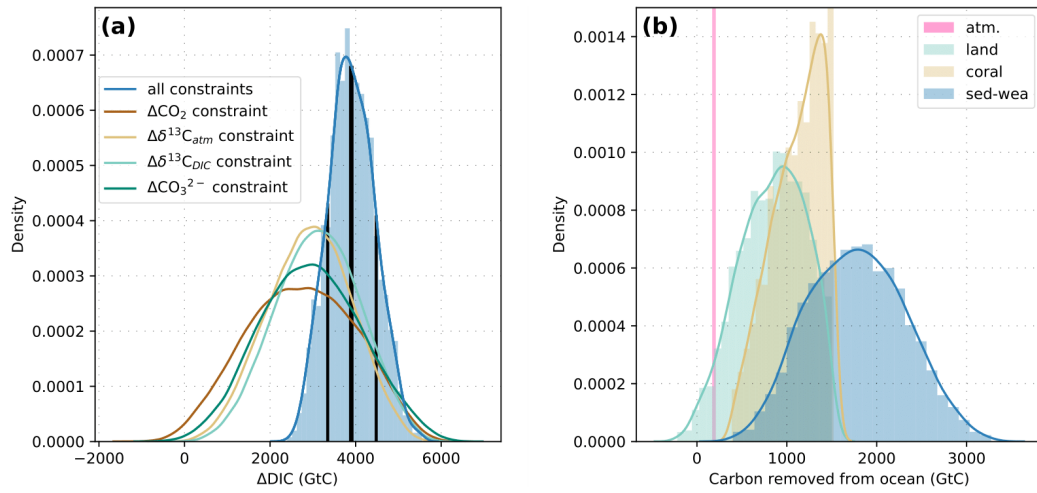


Figure S3 LGM-PI multi-constraint Δ DIC determined using the Bern3D model. The (a) total estimate and (b) contributions from atmosphere, land, coral and sedimentation-weathering imbalances.

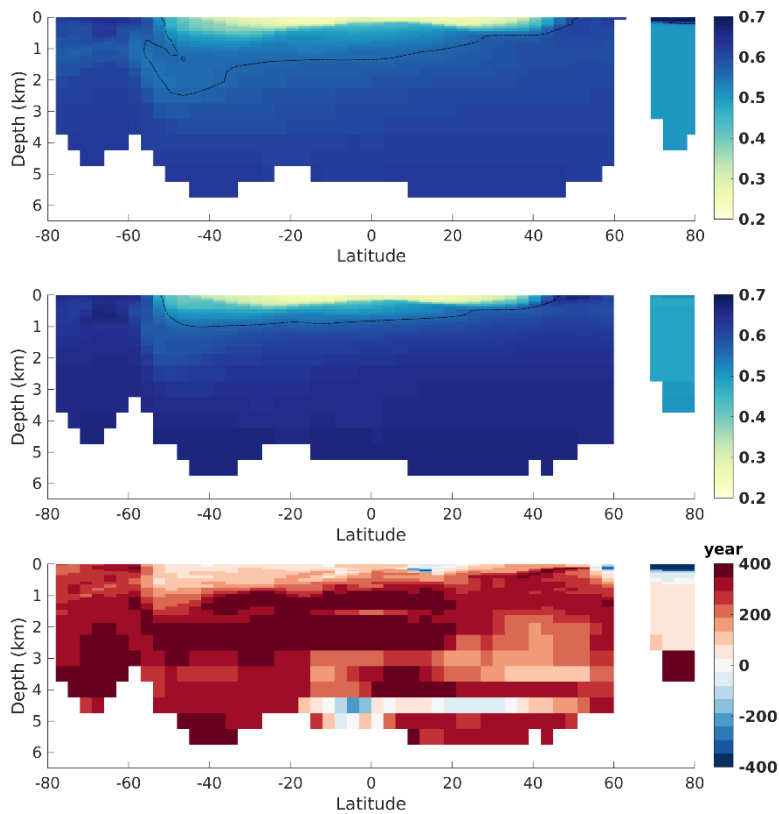


Figure S4 PO tracer Pacific zonal mean transect for the PI (top) and LGM (middle) simulation as well as Pacific change in radiocarbon age (bottom), as Fig. 1.

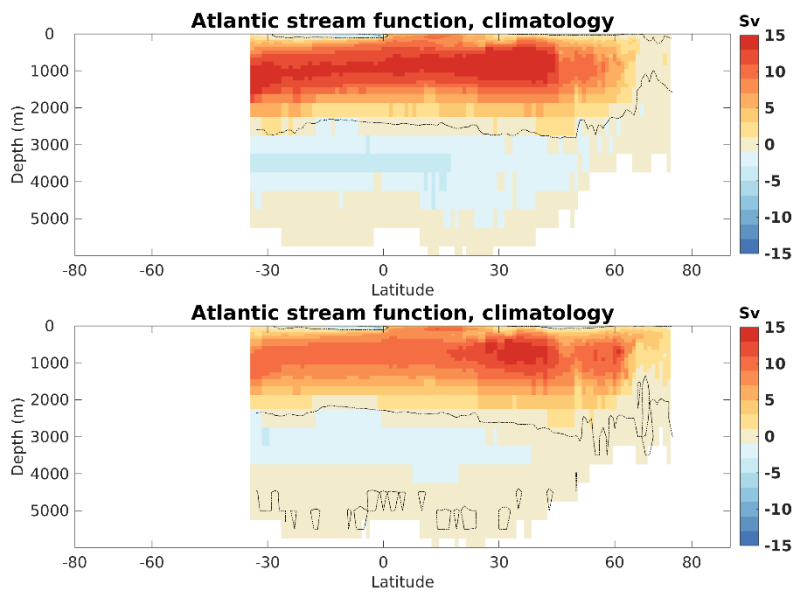


Figure S5 Atlantic stream functions for the PI (top) and LGM (bottom). The depth of the transition between the Atlantic overturning cells, as indicated by the depth of the zero Sv contour at 30°S, shallowed by ~350 m in our LGM setup as compared to the PI spinup.

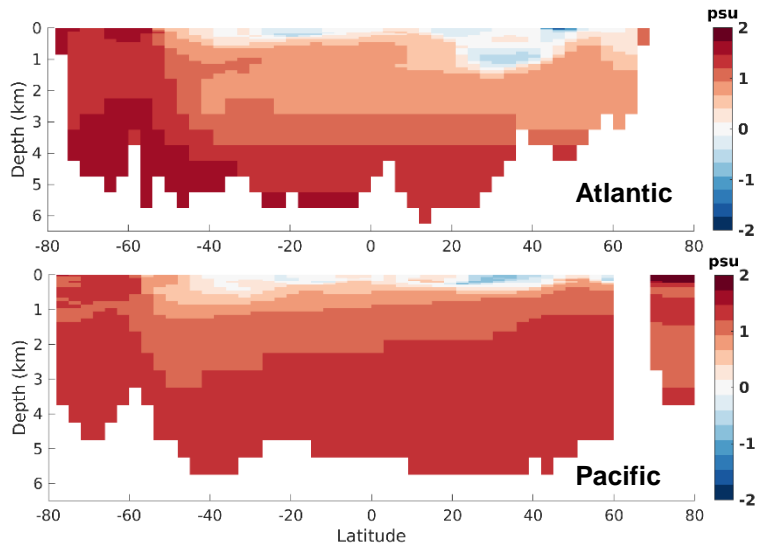


Figure S6 Simulated LGM-PI change in salinity.

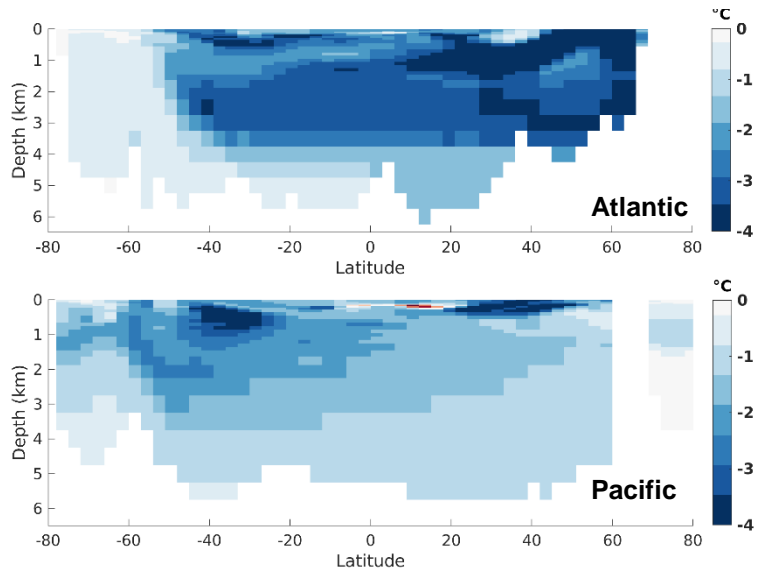


Figure S7 Simulated LGM-PI change in temperature.

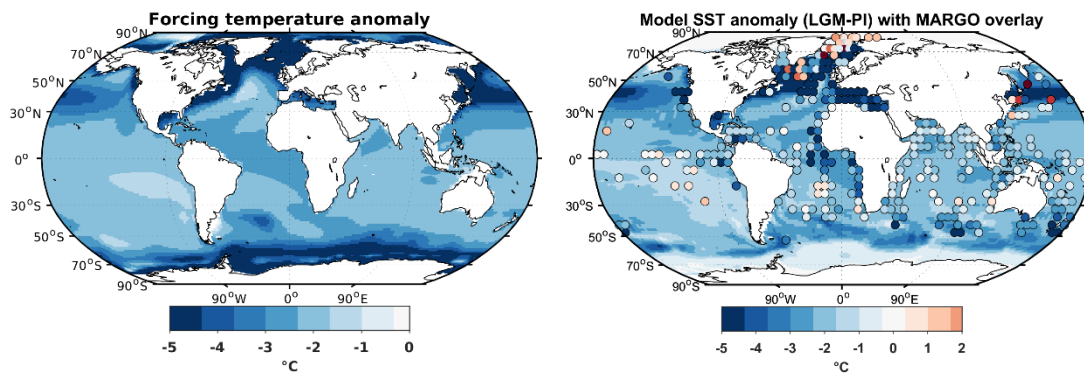


Figure S8 Atmospheric forcing (annual mean) (left) and simulated SST anomaly (right) with overlay of MARGO SST reconstruction data (Margo Project Members, 2009)

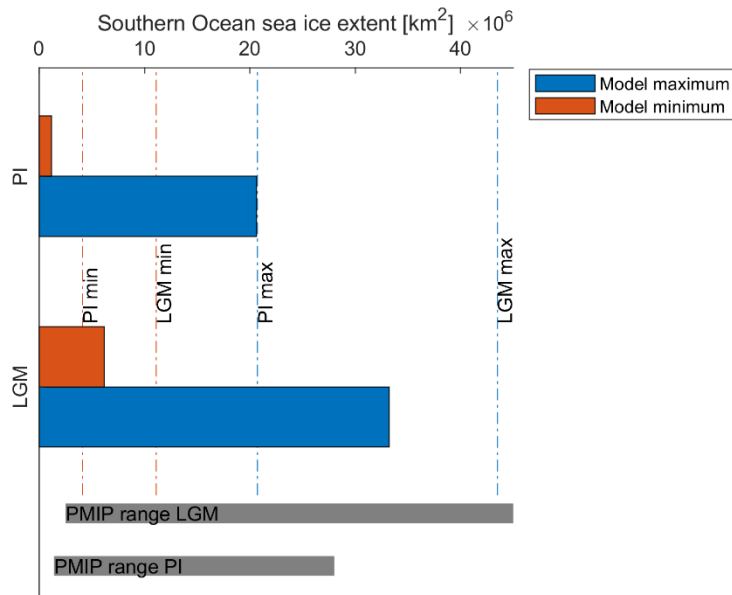


Figure S9 Southern Ocean sea ice extent (area of sea ice with a concentration of >15%) for the PI and LGM simulations. PMIP and observational estimate data from Roche et al. (2012) and Marzocchi and Jansen (2017).

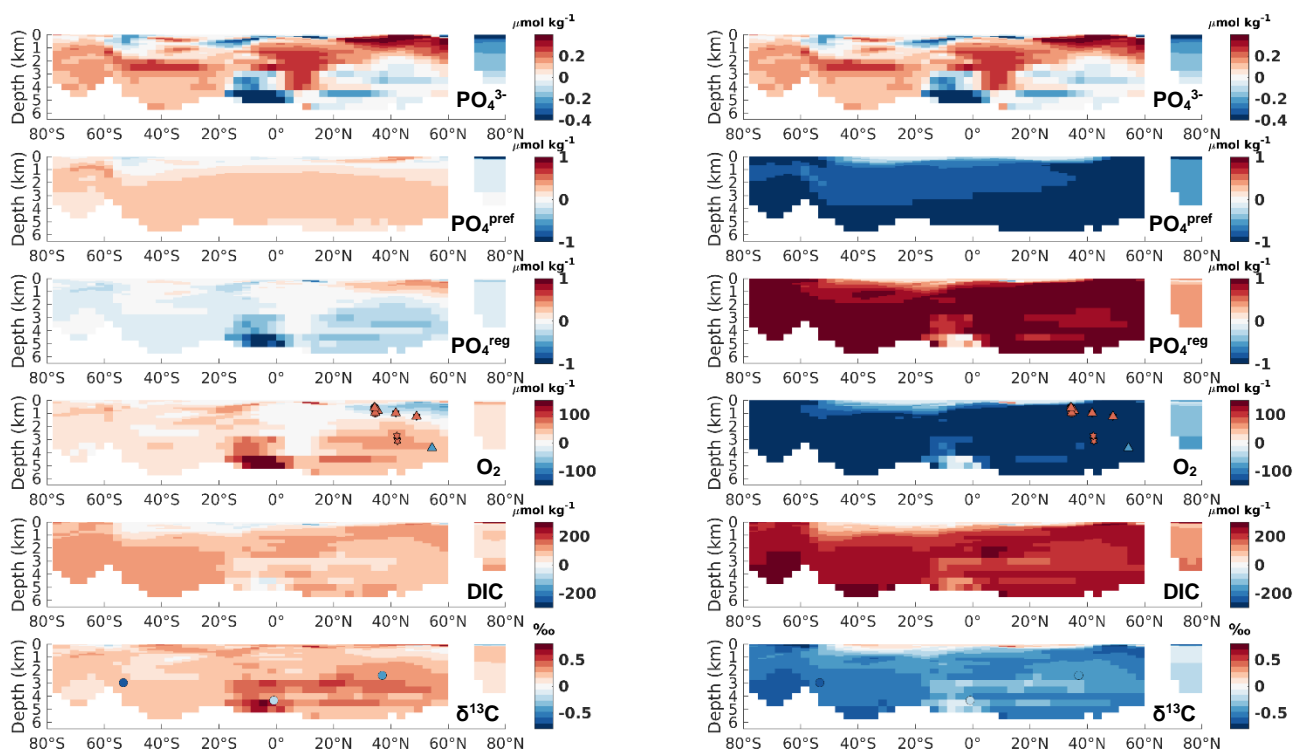


Figure S10 Pacific LGM-PI changes for the original model output (left-hand column) and adjusted to a biological pump efficiency of 75% (right-hand column). Otherwise as in Fig. 2 and 5.

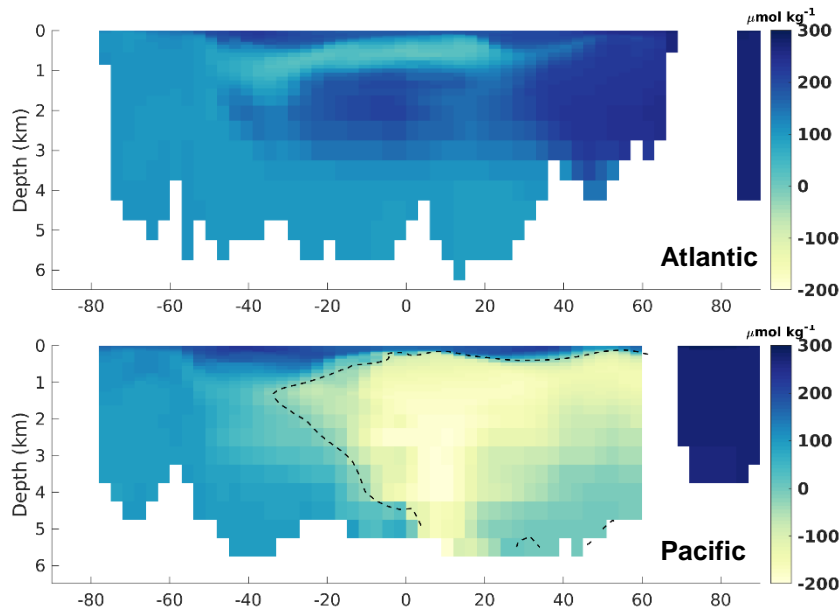


Figure S11 Simulated LGM O₂ concentrations for a 75 % $\overline{BP_{eff}}$, with a zero contour line.

References

- Jeltsch-Thömmes, A., Battaglia, G., Cartapanis, O., Jaccard, S. L., and Joos, F.: Low terrestrial carbon storage at the Last Glacial Maximum: constraints from multi-proxy data, *Climate of the Past*, 15, 849-879, 10.5194/cp-15-849-2019, 2019.
- Kleypas, J. A.: Modeled estimates of global reef habitat and carbonate production since the last glacial maximum, *Paleoceanography*, 12, 533–545, 10.1029/97PA01134, 1997.
- Marzocchi, A., and Jansen, M. F.: Connecting Antarctic sea ice to deep-ocean circulation in modern and glacial climate simulations, *Geophysical Research Letters*, 44, 6286-6295, 10.1002/2017GL073936, 2017.
- Milliman, J. D.: Production and accumulation of calcium carbonate in the ocean: budget of a nonsteady state, *Global Biogeochemical Cycles*, 7, 927–957, 1993.
- Morée, A., and Schwinger, J.: Last Glacial Maximum minus pre-industrial anomaly fields for use in forced ocean modelling, based on PMIP3 [Dataset]. Norstore, 2019a.
- Morée, A. L., and Schwinger, J.: A Last Glacial Maximum forcing dataset for ocean modelling, *Earth Syst. Sci. Data Discuss.*, 2019, 1-14, 10.5194/essd-2019-79, 2019b.
- Ridgwell, A. J., Watson, A. J., Maslin, M. A., and Kaplan, J. O.: Implications of coral reef buildup for the controls on atmospheric CO₂ since the Last Glacial Maximum, *Paleoceanography*, 18, 7 pp., 10.1029/2003PA000893, 2003.
- Roche, D. M., Crosta, X., and Renssen, H.: Evaluating Southern Ocean sea-ice for the Last Glacial Maximum and pre-industrial climates: PMIP-2 models and data evidence, *Quaternary Science Reviews*, 56, 99-106, <https://doi.org/10.1016/j.quascirev.2012.09.020>, 2012.
- Vecsei, A. and Berger, W. H.: Increase of atmospheric CO₂ during deglaciation: Constraints on the coral reef hypothesis from patterns of deposition, *Global Biogeochemical Cycles*, 18, 1–7, 10.1029/2003GB002147, 2004.